Francisco López Jiménez
Postdoctoral Researcher
Laboratoire de Mécanique des Solides,
École Polytechnique,
91128 Palaiseau, France
e-mail: lopez@lms.polytechnique.fr

Sergio Pellegrino
Joyce and Kent Kresa Professor of Aeronautics
and Professor of Civil Engineering,
California Institute of Technology,
1200 E. California Blvd,
MC 301-46, Pasadena, CA 91125
e-mail: sergiop@caltech.edu

Failure of Carbon Fibers at a Crease in a Fiber-Reinforced Silicone Sheet

Thin sheets of unidirectional carbon fibers embedded in a silicone matrix can be folded to very high curvatures, as elastic microbuckles with a half-wavelength on the order of 1 mm decrease the maximum strain in the fibers near the compression surface. This paper shows that probabilistic failure models derived from tension tests on individual fibers can be used to predict accurately the value of the outer surface curvature of the sheet, at which a small percentage of fibers break when a crease is formed in the sheet. The most accurate results are obtained by using a strain-based Weibull distribution of the failure probability in tension. [DOI: 10.1115/1.4007082]

1 Introduction

Carbon fiber composites are attractive for aerospace applications due to their high stiffness to density ratio and their high thermal stability, but their applicability to deployable structures has been limited by their brittle behavior. Recently, an alternative type of composite material has been developed, in which the fibers are embedded in a matrix that is many orders of magnitude softer than the fibers. It has been shown that deployable structures made of these materials can be packaged tightly. Examples of structures based around this approach are the elastic memory composite hinges developed by Francis et al. [1], where the carbon fibers are embedded in a shape-memory polymer, and the deployable reflector concept proposed by Datashvili et al. [2], consisting of a triaxial-weave carbon fiber fabric with a silicone matrix. A striking property is that localized creases can be introduced in thin sheets of these materials, leaving little or no damage when the creases are removed. Murphey et al. [3] have explained that the fibers in the compression region of the sheet form a series of elastic microbuckles and, through this mechanism, they can be subjected to a large geometric strain, while the material strain in the fibers is actually relatively small. The present authors [4] have recently shown that the shearing of the matrix between the fibers induces such high strains and, hence, damage in the matrix and/or matrix-fiber interface that the bending stiffness of the composite sheet significantly decreases when the sheet is subjected to cyclic bending.

However, one important effect that has yet to be understood is the onset of failure in the fibers. A simple estimate of the maximum bending strains in the most heavily buckled fibers, based on estimated buckle wavelength and amplitude combined with the tensile failure strain of the fibers, leads to vastly over-conservative predictions. We show in this paper that, by adopting a Weibull-type probabilistic description of the brittle failure of carbon fibers under pure tension, one can estimate quite accurately their failure curvature probability. We apply these results to the folding of composites of uniaxial carbon fibers in a silicone matrix and obtain accurate estimates for the probability of fiber failure for different degrees of tightness of the fold.

The layout of the paper is as follows. Following a review of the relevant literature in Sec. 2, Sec. 3 obtains analytical expressions for the probability of failure of carbon fibers in bending. Sections 4 and 5 present the results of tensile and bending tests on HexTow AS4 carbon fibers; it is shown that the probability distribution obtained from the tension tests can be used to generate, with good accuracy, the failure probability distribution for the bending tests. These results are then applied in Sec. 6 to composite sheets of unidirectional AS4 fibers in a silicone matrix; the predictions obtained from our theory are compared with experimental observations. Section 7 summarizes our findings and concludes the paper.

2 Background

Carbon fibers are brittle materials whose strength is controlled by the distribution and size of flaws. The failure process, known as the Reynolds-Sharp mechanism [5], consists of an initial flaw forming a crack that is driven by the shear stress acting on misoriented graphite planes [6]. Because of the variation in flaw size and the orientation of graphite planes, there is considerable spread in the tensile strength of carbon fibers, and so standard weak link theory is used to model their probability of failure [7]. The failure probability P of a fiber subject to uniform tensile stress σ is given by the Weibull distribution

$$P(\sigma, V) = 1 - \exp\left(-\frac{V}{V_0}\left(\frac{\sigma}{\sigma_0}\right)^m\right) \tag{1}$$

where V is the volume of the fiber, V_0 is the volume of the fiber used to characterize the material, σ_0 is a reference stress for which a fiber of volume V_0 has a probability of failure of $P = 1 - \exp(-1) \approx 0.632$, and m is the Weibull modulus, whose value controls the spread of strength variation. For carbon fibers, m usually lies between 3 and 8 [8,9]; the values of m have been increasing through the years as a result of improvements in fiber manufacturing.

The failure of fibers subject to bending was first studied by Sinclair [10], who introduced a test that consists in forming a loop with a single fiber and then pulling the ends until the fiber fails. Sinclair's original test measured the shortening of the fiber, which was then related to curvature by assuming that the shape of the looped fiber is given by the elastica. Sinclair's tests on glass fibers showed that the tensile strength under bending (defined as the maximum stress in the outermost surface of the fiber) is typically more than double the tensile strength under pure tension.

The Sinclair loop test has become one of the standard ways to test the bending properties of fibers. Due to the difficulty of performing a pure compression test [11], it is also used to analyze their compression behavior. The response during the loop test often shows softening at large strains [12], and Jones and Johnson

Contributed by Applied Mechanics of ASME for publication in the JOURNAL OF APPLIED MECHANICS. Manuscript received November 5, 2011; final manuscript received April 9, 2012; accepted manuscript posted July 6, 2012; published online November 19, 2012. Editor: Robert M. McMeeking.

[13] showed that the shape of the fibers during the test deviates from the shape predicted by the elastica, due to softening at large curvatures. This nonlinearity differs from the observations in Ref. [14], and it is usually explained as the result of buckling of the graphite layers on the compression side of a fiber. Its dependence on the type of fiber precursor, heat treatment temperature, and microstructure has been extensively studied [15–18]. Observations of a shift in the neutral axis of bending using X-ray diffraction [19] have confirmed that the two moduli have different values, with the ratio between the two varying greatly, depending on the type of fiber.

Studies of the flexural failure of carbon fibers have focused on the mean and standard deviation of properties, such as the maximum bending stress or strain. Recent studies [20,21] have characterized the failure probability of several types of carbon fiber under three-point bending or the loop test using Weibull distributions, but the connection between tensile and flexural failure of carbon fibers has not been investigated.

Turning to the behavior of thin sheets of uniaxial carbon fibers embedded in a soft matrix, analytical expressions for estimating the wavelength and amplitude of the microbuckled fibers were obtained by Francis et al. [22,23]. These authors assumed that the buckles can be described by the sine function

$$y = a \sin \frac{\pi x}{\lambda} \tag{2}$$

where a is the amplitude and λ the half-wavelength, defined as corresponding to a phase of π radians. They determined the following expression for the initial buckle wavelength λ_0 from energy considerations, assuming plane sections to remain plane. They also assumed the fibers to have a circular cross-section with radius R and to be arranged according to a square lattice with spacing $b = R\sqrt{\pi/V_f}$ and obtained

$$\lambda_0 = \left(\frac{9\pi^3 V_f t^2 EI}{8R^2 \log\left(\frac{3t}{b}\right) G} \right)^{\frac{1}{4}} \tag{3}$$

where V_f is the fiber volume fraction, t the thickness of the sheet, E and I the modulus and second moment of area of the fibers, and G the shear modulus of the matrix.

3 Analysis of Failure Probability in Bending

When the stress is not uniform and it is reasonable to assume that failure in compression is ductile, the probability of failure is obtained by integration of Eq. (1) over the volume, where σ is tensile, V_t,

$$P = 1 - \exp\left(-\frac{1}{\sigma_0^m V_0} \int_{V_t} \sigma^m dV \right) \tag{4}$$

It should be noted that the assumption of ductile behavior in compression is based on a somewhat simplified interpretation of the body of existing evidence, which indicates that compressive failure depends on the type of fiber and the manufacturing process [11,18,24].

Consider a circular fiber of radius R and total length L subject to a bending curvature $\kappa = \kappa(s)$. Assuming the stress-strain relationship to be linear in the tensile region, the curvature and tensile stress are related by

$$\sigma = E_t \kappa \eta \tag{5}$$

where η is the distance from the neutral axis and E_t the tensile modulus. Substituting into Eq. (4) gives

$$P = 1 - \exp\left(-\frac{1}{\sigma_0^m V_0} \int_0^L \int_{A_t} (E_t \kappa(s) \eta)^m dA ds \right) \tag{6}$$

where A_t is the area of section under tension.

Next, it is assumed that the position of the neutral axis does not depend on κ. Hence, the two integrals in Eq. (6) can be evaluated independently and so the probability of failure is expressed as

$$P = 1 - \exp\left(-\frac{2}{m+1} \frac{(E_t \kappa_{\max})^m}{\sigma_0^m V_0} I_1 I_2 \right) \tag{7}$$

where $\kappa_{\max}$ is the maximum curvature along the fiber and the quantities I_1, I_2 are defined as

$$I_1 = \int_0^L \left| \frac{\kappa(s)}{\kappa_{\max}} \right|^m ds \tag{8}$$

$$I_2 = \int_0^{\xi_n} \left(\sqrt{R^2 - \xi^2} - \eta_n \right)^{m+1} d\xi \tag{9}$$

where η_n and ξ_n define the position of the neutral axis (see Fig. 1).

The value of I_1 depends only on the curvature of the fiber and the value of the Weibull modulus m. There are several situations in which $\kappa(s)$ scales with $\kappa_{\max}$, and so the ratio $\frac{\kappa(s)}{\kappa_{\max}}$ is a particularly convenient choice. This is the case for the fiber loop test and the three-point bending test, two common experiments used to calculate the failure properties of carbon fibers under bending, as well as for the case of fiber microbuckling in composites with a soft matrix. The value of I_2 has a constant value for a given type of fiber.

Note that the above analysis does not require the neutral axis to pass through the center of the fiber. If the tensile and compressive moduli, E_t, E_c, have different (but constant) values, we can solve for (ξ_n, η_n) as a function of E_t/E_c by setting the axial force resultant equal to zero, which leads to

$$\frac{\pi}{2}\left(1 - \frac{E_t}{E_c}\right) + \left[\arcsin\left(\frac{\eta_n}{R}\right) + \frac{\eta_n \xi_n}{R^2} \right]\left(1 + \frac{E_t}{E_c}\right) = 0 \tag{10}$$

with

$$\xi_n^2 + \eta_n^2 = R^2 \tag{11}$$

For example, values of $\frac{E_t}{E_c}$ equal to 1.5, 2, and 5 correspond to a shift of the neutral axis by 0.16, 0.27, and 0.59 times the radius, respectively.

4 Tensile Failure of AS4 Fibers

The failure probability in the tension of AS4 fibers has been investigated. AS4 is a polyacrylonitrile (PAN)-based, high

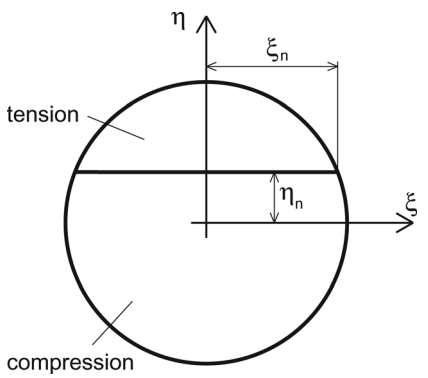

Fig. 1 Position of neutral axis in the fiber cross section for $E_t > E_c$

strength, high strain fiber produced by Hexcel. Its properties are given in Table 1.

A total of 99 fibers with a gauge length $L = 20$ mm were tested following the American Society for Testing and Materials (ASTM) D 3379-89 standard (see also Ref. [25]), using an Instron 5569 testing machine with a 10-N load cell. Retro-reflective strips were attached at the ends of the gauge length to measure the fiber strain with an Epsilon LE01 laser extensometer. A uniform displacement rate of 0.5 mm/min was applied until the fiber failed.

Figure 2(*a*) shows a plot (with the natural logarithm of the failure probability on the vertical axis) of the results obtained from these tests. The stress at failure, obtained by dividing the maximum force by the fiber cross-sectional area (assuming a diameter of exactly 7.1 μm; see Table 1) has been normalized by σ_0, calculated as explained in Sec. 2. The reference volume V_0 was calculated as $\pi R^2 L = 7.92 \times 10^{-4}\text{mm}^3$. The probability of failure P_i for the i-th strength was estimated from [26]

$$P_i = \frac{i - 0.5}{N} \tag{12}$$

where N is the sample size. Two test results were discarded as clear outliers.

A Weibull distribution, Eq. (1), was then fitted to the experimental results using least squares to obtain the Weibull modulus $m = 8.86$ and reference stress $\sigma_0 = 4.68$ GPa.

Table 1 AS4 properties provided by Hexcel

Longitudinal tensile modulus, E_t	231 GPa
Tensile strength	4.433 GPa
Tensile failure strain, ε_f	1.8%
Radius, R	3.55 μm

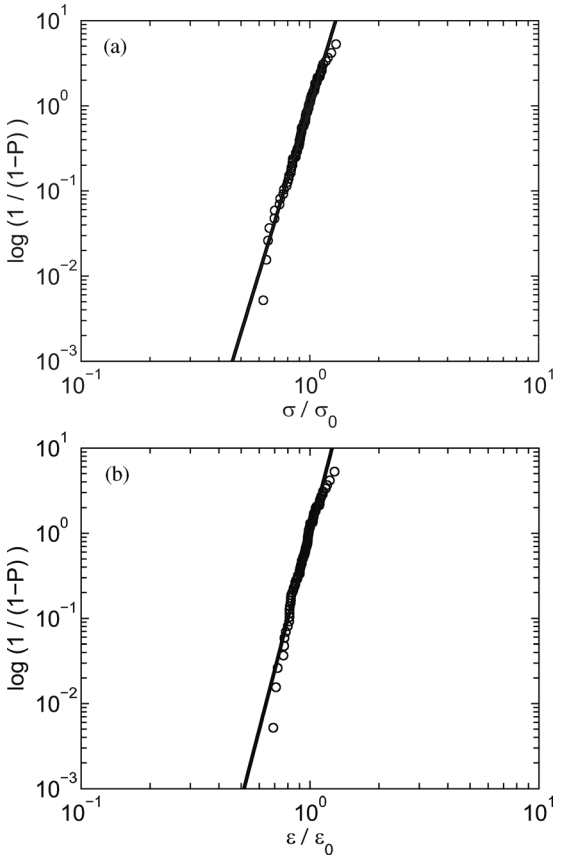

Fig. 2 Weibull fit to probability of tensile failure for AS4 fibers versus (*a*) applied stress and (*b*) strain

An alternative approach is to consider the strain at failure, which is a more direct outcome of the experiments, and to determine the Weibull modulus for the probability of failure in terms of strain. Then, Eq. (1) becomes

$$P(\varepsilon, V) = 1 - \exp\left(-\frac{V}{V_0}\left(\frac{\varepsilon}{\varepsilon_0}\right)^{m'}\right) \tag{13}$$

Both the experimental results and the Weibull fit have been plotted in Fig. 2(*b*), and it is interesting to note that, in this case, the Weibull modulus is $m' = 10.397$ with $\varepsilon_0 = 1.898$.

The discrepancy between the two approaches can be explained by noting that the longitudinal modulus of each fiber, defined as the ratio between stress and strain at failure, has an average value of 237.61 GPa, with a standard deviation of 6.96%. Since the actual modulus is unlikely to vary to such an extent, a more likely explanation is that the calculation of the failure stress is affected by variations in the fiber diameter, whereas the failure strain has been measured directly. It should be noted that a variation of 5% in fiber diameter would explain a variation of up to 10% in the calculated stiffness. This range of values agrees with the standard deviation of the fiber diameter, which typically ranges from 3.07% to 7.66% [9].

5 Bending Failure of AS4 Fibers

In this section, we compare the failure probability in bending, obtained by carrying out direct loop tests on individual fibers, with predictions based on the approach presented in Sec. 3.

5.1 Loop Tests. The bending failure tests followed a procedure similar to the Sinclair loop test [10]. A loop was formed with a single fiber and was placed between two glass surfaces lubricated with a drop of light mineral oil. One end of the loop was held fixed, while the other end was attached to a slider. Moving the slider had the effect of increasing the distance between the two ends; thus, increasing the curvature of the loop. The tests were performed under a Nikon Eclipse LV100 microscope with a Nikon DS-Fi1 digital camera. A video of the complete test was recorded, and the last frame before failure was used to calculate the radius of curvature at failure, r_f, by computing the least-squares best fit to several points near A in Fig. 3. This test was done on 58 fibers.

It should be noted that the curvature at failure is not exactly $\frac{1}{r_f}$, since the test configuration permits an out-of-plane displacement of the fiber; hence, the shape of the fiber at failure is helical. The pitch of the helix at the point of highest curvature is approximately h/π, where h is the vertical distance between points B and B'. This distance can be measured by focusing the microscope on either B or B', and it was found to be approximately 50 μm. Hence, the failure curvature is given by

$$\kappa = \frac{r_f}{r_f^2 + (h/\pi)^2} \tag{14}$$

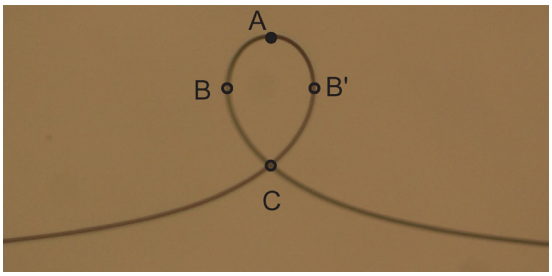

Fig. 3 Example of image used to measure r_f

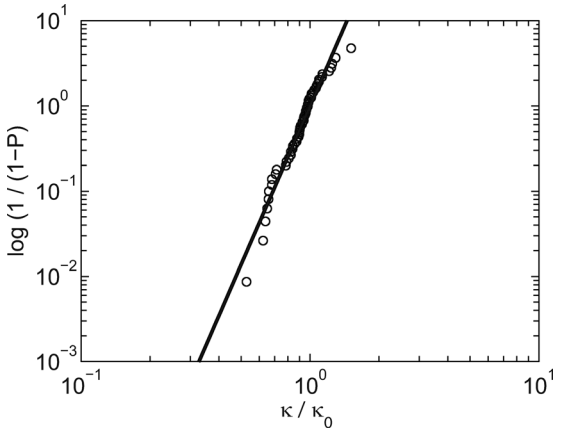

Fig. 4 Weibull fit of probability of failure in bending versus applied curvature for AS4 fibers; $\kappa_0 = 12.349\ \text{mm}^{-1}$

Two important differences between the loop test and the tensile test should be mentioned. First, the curvature is not constant along the fiber and, hence, the failure curvature has been defined as the measured maximum curvature of the fiber. Second, the test configuration determines its own intrinsic fiber length, which decreases as the maximum curvature increases. In other words, in the tension test, we could arbitrarily choose the specimen length, but here it is determined by the test itself.

Assuming these effects to be small, in Fig. 4, we have plotted the failure curvature normalized by $\kappa_0 = 12.349\ \text{mm}^{-1}$ versus the failure probability determined from Eq. (11). These results can be closely approximated with a straight line, indicating that a Weibull distribution with modulus $m_b = 6.182$ provides a reasonably accurate representation of the experimental results.

5.2 Analysis of Loop Test Results. PAN-based fibers of modulus similar to AS4 have a similar compressive and tensile elastic modulus [24]. Hence, it will be assumed that the neutral axis passes through the centroid, $\eta_n = 0$.

If it is further assumed that the two moduli remain constant at larger strains and hence that the two-dimensional solution for the shape of the fiber during the loop test is given by the elastica [27]. The shape of the elastica can be determined by integrating the following equations:

$$\frac{dt_1}{ds} = \kappa t_2 \tag{15}$$

$$\frac{dt_2}{ds} = -\kappa t_1 \tag{16}$$

$$\frac{dx}{ds} = t_1 \tag{17}$$

$$\frac{dy}{ds} = t_2 \tag{18}$$

where t_i is the i-th component of the tangent vector. Also,

$$\kappa = \frac{M}{EI} = \frac{F(H+y)}{EI} \tag{19}$$

where M is the bending moment, F the end force, and H the distance from the line of action of F to the point of maximum curvature (see Fig. 5). The values of H and F to form a stable loop (i.e., with $M = 0$, when $s \to \infty$) can be obtained from

$$H = \frac{4}{\kappa_{\max}} \tag{20}$$

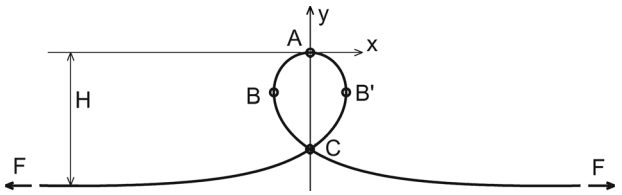

Fig. 5 Elastica

$$F = \frac{\kappa_{\max}^2 EI}{4} \tag{21}$$

$\kappa(s)$ was computed from the values of $x(s)$ and $y(s)$ that had been obtained by numerical integration of Eqs. (15)–(18); it has been plotted in Fig. 6(*a*). Figure 6(*b*) shows plots of the integral I_1, calculated from Eq. (8) for different values of m_b. This plot shows that I_1 converges much faster than κ decays and so, since in the present case $m_b = 6.18$, a good accuracy could be achieved by integrating only up to point B.

The probability of failure in the loop test can be calculated as a function of the maximum curvature, $\kappa_{\max}$, using Eq. (7), with the value of I_1 obtained as above and I_2 obtained from Eq. (9).

The experimental results in Fig. 2 have been replotted in Fig. 7 together with the analytical predictions obtained in the way described above and using both the stress-based, m, and strain-based, m', Weibull moduli obtained from the tension tests. Three vertical lines have been added to the plot for reference. They correspond to the curvatures at which the maximum strain in the fibers is ε_f, $1.5 \times \varepsilon_f$, and $2.0 \times \varepsilon_f$, where $\varepsilon_f = 1.8\%$ is the mean tensile failure strain given by the manufacturer. Note that the first vertical line, $\kappa = 5.07\text{mm}^{-1}$, occurs well before any bending failures are actually observed.

The distribution of experimental results in Fig. 7 show non-smoothness as well as jumps, particularly in the range $P = 0 - 20\%$. These discontinuities are attributed to the fact that the loop tests require more manipulation of the fibers than the tensile test, which results in some fibers failing prematurely. Overall, both sets of predictions provide an accurate estimate of the maximum curvature for small values of the failure probability. The strain-based Weibull modulus, m', provides a much closer fit to the full range of experimental measurements, thus confirming the conjecture made in Sec. 4 that the strain-based modulus captures more accurately the actual diameter of the fibers.

It is concluded that the Weibull moduli for tensile failure provide good predictions for the probability of bending failure in the loop test, with m' providing a more accurate description of the

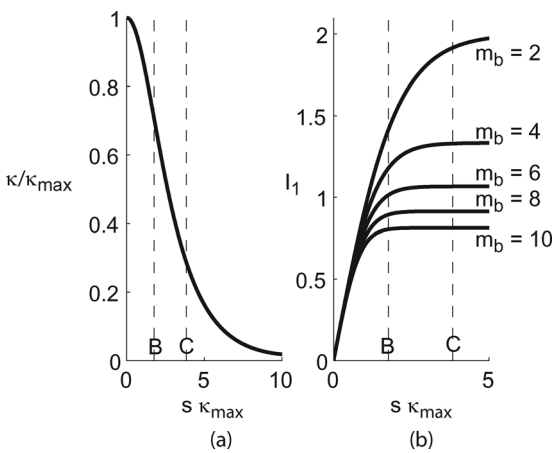

Fig. 6 Curvature κ and value of I_1 for different values of m as a function of the arc length s

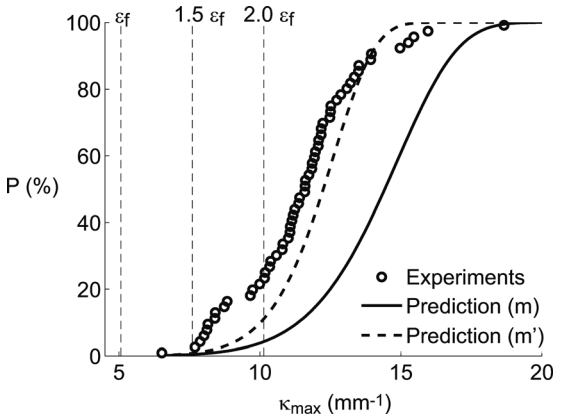

Fig. 7 Failure probability versus maximum curvature for loop test; the two sets of predictions are based on the stress- and strain-based Weibull moduli for tensile failure

probability distribution. In Sec. 6, they will be used to carry out an analysis of the failure probability of fibers at a localized crease in thin sheets of fiber-silicone composites.

6 Creasing of Composite Sheets

This section applies the results of Sec. 5 to the study of fiber failure at a crease in a thin sheet made of unidirectional fibers embedded in a silicone matrix. The macroscopic curvature at which the fibers in the sheet begin to fail is measured experimentally and then compared to the predictions.

6.1 Experiments. The sheets used in these experiments were produced by L'Garde using 12 K unidirectional tows of AS4 fibers and a silicone rubber with initial elastic modulus of 1 MPa and shear modulus of 0.27 MPa. The sheets had a thickness of 0.54 mm and a fiber volume fraction $V_f = 35\%$. For this particular combination of materials and fiber volume fraction, microbuckling starts at very low curvatures of the sheet and the initial wavelength is $\lambda_0 \approx 1.5$ mm. As the sheet is folded more tightly, the amplitude of the buckles increases and the wavelength decreases. A view of the buckled fibers is shown in Fig. 8.

In order to determine a quantitative relation between curvature and fiber damage, 18 strips with a width of 5 mm were folded under a Nikon ShuttlePix digital microscope. From the images, the curvature of the outer (tensile) surface of the strip could be measured (see Fig. 9(*a*)). As the curvature increases, the geometry of the outer surface tends to deviate from a cylinder, as the outer edges of the sheet form a three-dimensional curve with maximum curvature higher than the rest of the sheet. However, these higher curvatures occur only in a relatively small boundary layer (see Fig. 9(*b*)) and were not measured, because failure is usually observed away from the edges.

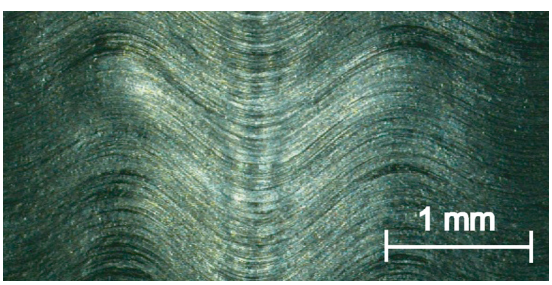

Fig. 8 Fiber microbuckling on compression side of 0.54-mm-thick sheet

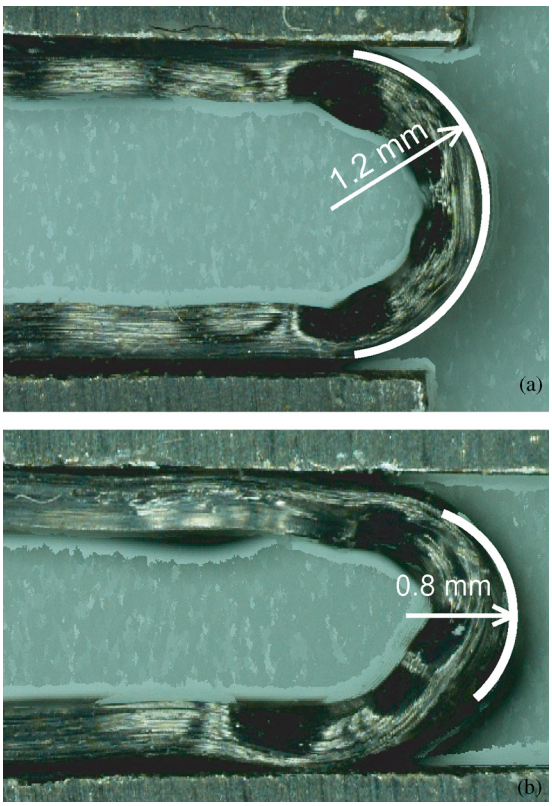

Fig. 9 Examples of curvature measurement: (*a*) $\kappa = 0.83$ mm^{-1}; (*b*) $\kappa = 1.25$ mm^{-1} showing also edge waviness

After the specimens had been folded, they were flattened and the compression side was observed under a Nikon Eclipse LV100 microscope to look for broken fibers. The length of each line of broken fibers (see Fig. 10) was measured and compared to the total width of the strip to obtain the percentage of fibers on the compressive surface that had failed under the applied curvature. No attempt was made to observe if any internal fibers had failed.

6.2 Analysis. It has been shown in Sec. 5.2 that, in the case of the loop test, the probability of bending failure of the Hexcel AS4 fibers can be computed with Eq. (7). Since the same fibers have been used to construct the strips tested in Secs. 4 and 5, the same approach can be used to estimate the probability of failure of the fibers in the strips.

The integral I_1 in Eq. (8) has to be calculated for the buckled shape of the fibers given by E. (2) [22,23]. The length of fiber in

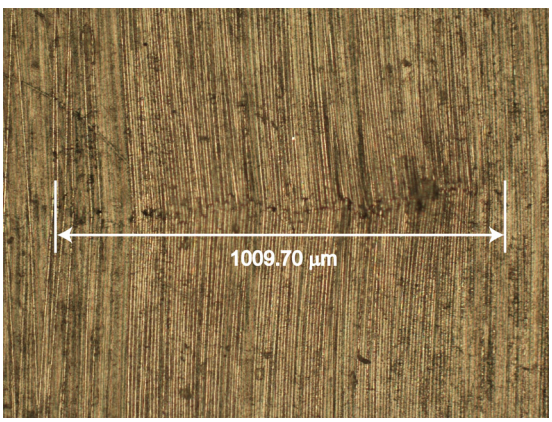

Fig. 10 Measurement of broken fibers after creasing

the crease can be expressed as $L = n\lambda$, where n is the number of buckles to be considered and λ is the half-wavelength of the buckled fiber. To calculate I_1, we express κ and ds as

$$\kappa = \frac{y''}{[1 + (y')^2]^{\frac{3}{2}}} \tag{22}$$

$$ds = [1 + (y')^2]^{\frac{1}{2}} dx \tag{23}$$

where $()' = d()/dx$. The maximum curvature of the fiber is given by

$$\kappa_{\max} = \frac{a\pi^2}{\lambda^2} \tag{24}$$

and finally we introduce the variable $\hat{x} = \frac{x}{\lambda}$. Hence, I_1 is calculated as follows:

$$\begin{aligned} I_1 &= \int_0^L \frac{\left|\sin\frac{\pi x}{\lambda}\right|^m}{\left(1 + \left(\frac{a}{\lambda}\pi\cos\frac{\pi x}{\lambda}\right)^2\right)^{\frac{3m}{2}}} ds \\ &= n\lambda \int_0^1 \frac{|\sin \pi\hat{x}|^m}{\left(1 + \left(\frac{a}{\lambda}\pi\cos\pi\hat{x}\right)^2\right)^{\frac{3m-1}{2}}} d\hat{x} \end{aligned} \tag{25}$$

It should be noted that this integral depends only on m, λ, and a. The value of m has already been determined in Sec. 5; the latter two parameters are a function of the applied curvature and can be determined as follows.

To determine λ, we will assume, for simplicity, the extreme case, where the neutral surface coincides with the tension surface of the creased sheet. Consider the deformation of a sheet of initial length λ_0. Assuming plane sections to remain plane (an assumption consistent with Refs. [22] and [23]), the half wavelength of the buckled fibers on the compression side of the sheet is equal to (see Fig. 11)

$$\lambda = \lambda_0(1 - \kappa t) \tag{26}$$

where λ_0 is obtained from Eq. (3).

Once λ is known, a can be calculated by assuming that the buckled fibers do not carry any axial force, and hence, their axial length is constant. This yields the equation

$$\int_0^1 \sqrt{1 + \left(\frac{a}{\lambda}\pi\cos\pi\hat{x}\right)^2}\, d\hat{x} = \frac{1}{1 - \kappa t} \tag{27}$$

which can be solved for a.

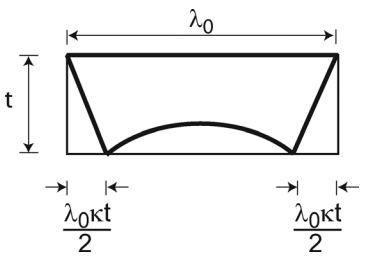

Fig. 11 Kinematics of bending deformation for a segment of composite sheet of initial length λ_0, subject to a curvature κ. The neutral surface is assumed to coincide with the tension surface.

Lastly, the number of buckled half-waves depends on both the wavelength of the microbuckles and the length of sheet over which the crease extends. Since, in the experiments, the imposed kink angle was π radians, n will be the first integer that satisfies the condition

$$n \geq \frac{\pi}{\kappa\lambda_0} \tag{28}$$

6.3 Results. We have predicted the probability of failure for a fiber that lies on the compression side of a sheet of thickness $t = 0.54$ mm with a crease of π radians. The predictions were obtained from Eq. (7) as follows. For the material used for our experiments, the initial wavelength $\lambda_0 = 1.57$ mm was obtained from Eq. (3). This value is in good agreement with the observed experimental wavelength reported in Sec. 6.1. Then, for any given curvature κ, Eqs. (19) and (20), respectively, provided the values of λ and a. The value of I_1 was obtained from Eq. (18) and I_2 from Eq. (9).

The predicted probability of failure has been plotted in Fig. 12 together with the results from the tests described in Sec. 6.1. The model provides a good prediction for the curvature at which damage starts taking place, $\kappa \approx 0.9$ mm^{-1}, and also provides a good lower bound for the amount of damage as the curvature of the crease is increased.

The spread in experimental results in Fig. 12 may be due to the three-dimensional features of the fold and also to the fact that the failure of one fiber affects the state of neighboring ones.

6.4 More General Cases. The results presented thus far have been for a specific sheet, in order to demonstrate the accuracy achieved by the present model. Readers interested in potential applications of silicone-reinforced carbon fiber composites will want to know how tightly thin sheets of different thicknesses and with a variety of fiber and matrix properties can be packaged with little or no damage. Answers to such questions can be obtained from Fig. 13, where it has been assumed that a failure probability of 1% in the most compressed layer of fibers is acceptable. For any value of λ_0, which is computed from Eq. (3) for any given set of material/geometric properties of the sheet, this plot provides the value of κt and also the corresponding value of the maximum strain in the fibers, $\varepsilon_{\max}$, reached at the point of maximum curvature of the buckled fibers. In computing the probability of failure, it has been assumed that there is only one buckle, in order to eliminate the dependence on the thickness t, and the remaining parameters have been left unchanged from the previous study; in particular, we have used the strain-based Weibull modulus $m' = 10.397$.

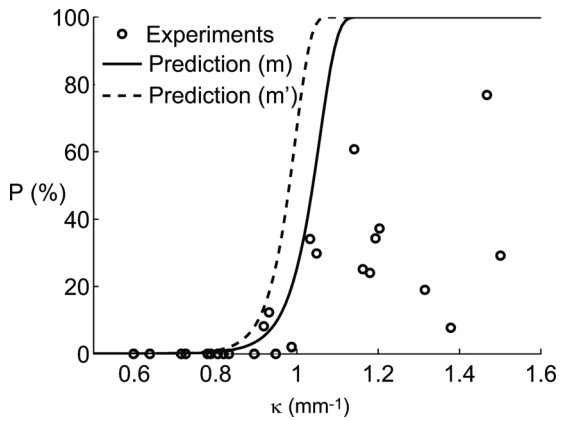

Fig. 12 Probability of failure for fibers on compression side of 0.54-mm-thick sheet with a fold of π radians with curvature κ

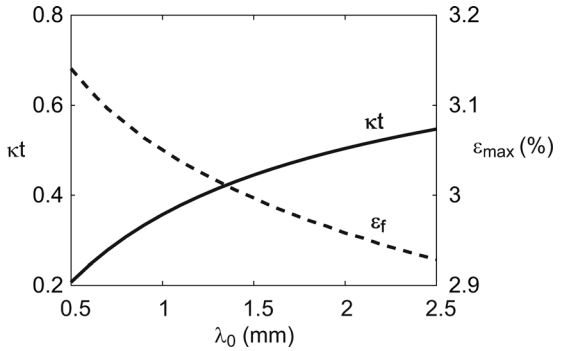

Fig. 13 Values of κt and ε_f for creases with a single buckle and a failure probability of 1%

In Fig. 13, it is interesting to note that the smallest value of $\varepsilon_{\max}$ is 2.93%, which is 63% higher than the failure strain of the fibers in Table 1.

7 Discussion and Conclusion

This paper has presented a study of the failure of carbon fibers, linking their failure probability under pure tension to failure under bending. The results of this study were applied to the creasing of thin sheets of composite materials of unidirectional fibers embedded in a silicone matrix. It has been shown that probabilistic failure models derived from tension tests on individual fibers can be used to predict accurately the outer surface curvature of the sheet at which a small percentage of fibers break when a crease is formed in the sheet.

The most accurate results were obtained using a strain-based Weibull distribution of the failure probability in tension, which, for the case of Hexcel AS4 fibers, was determined to have a modulus $m' = 10.397$. The corresponding failure probability for fibers under bending can be calculated from

$$P = 1 - \exp\left(-\frac{2}{m'+1}\frac{(E_t\kappa_{\max})^{m'}}{\sigma_0^{m'}V_0}I_1I_2\right) \tag{29}$$

where

$$I_1 = \int_0^L \left|\frac{\kappa(s)}{\kappa_{\max}}\right|^{m'} ds$$

$$I_2 = \int_0^{\xi_n} \left(\sqrt{R^2-\xi^2}-\eta_n\right)^{m'+1} d\xi$$

The validity of this approach was confirmed by comparing the maximum curvatures measured from loop tests on 58 fibers to predictions in which the failure probability was computed from Eq. (21), and the curvature of the fiber was assumed to vary according to an elastica curve.

The same probability distribution was then used to calculate the fiber failure probability in a composite sheet made of unidirectional carbon fibers in a silicone matrix. Assuming that the outer surface of the sheet does not stretch, the buckling wavelength and amplitude of the innermost fibers were estimated as functions of the curvature of the crease from Eqs. (19) and (20), with the initial buckling wavelength given by Eq. (3). With this assumption, and also assuming that a single buckle will be responsible for fiber failure, the integral I_1 has the expression

$$I_1 = \lambda\int_0^1 \frac{|\sin\pi\hat{x}|^{m'}}{\left(1+\left(\frac{a}{\lambda}\pi\cos\pi\hat{x}\right)^2\right)^{\frac{3m'-1}{2}}}d\hat{x} \tag{30}$$

Again, the validity of this approach was checked against direct measurements of percentages of failed fibers on the inner surface of thin sheets that had been creased by different amounts.

The results of the present study could have major implications in the design of space structures made of carbon-fiber silicone composites, as the results in Fig. 13 show that thin sheets made of these materials can be subjected to localized curvatures that are at least 63% higher than the curvature limits that would be calculated by using the failure strain of the fibers provided by the supplier, if it is accepted that only 1% of fibers on the most compressed surface of the sheet are allowed to break. It should also be noted that there are other cases in which unexpectedly high fiber strains have been observed in thin composite plates [28]; it may be possible to explain these observations by an approach analogous to that presented here.

Acknowledgment

We thank Dr. Thomas Murphey (AFRL) and Professor Zhigang Suo (Harvard University) for helpful comments and L'Garde Inc. for providing test samples.

Nomenclature

a = amplitude of fiber microbuckle
A = fiber cross-sectional area
A_c = area of fiber section under compression
A_t = area of fiber section under tension
E = Young's modulus
E_c = compressive Young's modulus of fiber
E_t = tensile Young's modulus of fiber
F = end force on looped fiber
G = shear modulus of matrix
h = out-of-plane distance between points of looped fiber
H = distance from line of action of F to point of maximum curvature of looped fiber
I = second moment of area of fiber
I_1, I_2 = integrals to calculate Weibull failure probability
L = length of fiber
m, m' = stress-, strain-based Weibull modulus of tensile failure
m_B = Weibull modulus of bending failure
M = bending moment
n = number of buckles in microbuckled fiber
N = sample size
P = probability of failure
R = fiber radius
r_f = fiber radius of curvature at failure
s = curvilinear coordinate along fiber
t = thickness of sheet
V = volume of tested fiber
V_0 = normalizing Weibull fiber volume
V_f = fiber volume fraction
ε = strain
ε_0 = normalizing Weibull strain
ε_f = fiber tensile failure strain
λ = half-wave length of fiber microbuckle
λ_0 = initial half-wave length of fiber microbuckle
κ = curvature of fiber, curvature of sheet
σ = stress
σ_0 = normalizing Weibull stress
ξ, η = coordinate system in fiber cross-section

References

[1] Francis, W., Lake, M. S., Mallick, K., Freebury, G. E., and Maji, A., 2003, "Development and Testing of a Hinge/Actuator Incorporating Elastic Memory Composites," 44th AIAA Structures, Structural Dynamics, and Materials Conference, Norfolk, VA, April 7–10, Paper No. AIAA 2003-1496.
[2] Datashvili, L., Baier, H., Wehrle, E., Kuhn, T., and Hoffmann, J., 2010, "Large Shell-Membrane Space Reflectors," 51st AIAA/ASME/ASCE/AHS/ASC Structures, Structural Dynamics, and Materials Conference, Orlando, FL, April 12–15, Paper No. AIAA 2010-2504.
[3] Murphey, T. W., Meink, T., and Mikulas, M. M., 2001, "Some Micromechanics Considerations of the Folding of Rigidizable Composite Materials," 42nd

AIAA/ASME/ASCE/AHS/ASC Structures, Structural Dynamics, and Materials Conference, Seattle, WA, April 16–19, Paper No. AIAA-2001-1418.
[4] López Jiménez, F., and Pellegrino, S., 2012, "Folding of Fiber Composites With a Hyperelastic Matrix," Int. J. Solids Struct., **49**, pp. 395–407.
[5] Reynolds, W. N., and Sharp, J. V., 1974, "Crystal Shear Limit to Carbon Fibre Strength," Carbon, **12**, pp. 103–110.
[6] Bennett, S. C., Johnson, D. J., and Johnson, W., 1983, "Strength-Structure Relationships in PAN-Based Carbon Fibres," J. Mater. Sci., **18**, pp. 3337–3347.
[7] Donnet, J. B., Wang, T. K., Peng, J. C. M., and Rebouillat, S., 1998, *Carbon Fibers*, 3rd ed., Marcel Dekker, New York.
[8] Bader, M. G., Pickering, K. L., Buxton, A., Rezaifard, A., and Smith, P. A., 1993, "Failure Micromechanisms in Continuous Carbon-Fibre/Epoxy-Resin Composites," Compos. Sci. Technol., **48**, pp. 135–142.
[9] Naito, K., Tanaka, Y., Yang, J.-M., and Kagawa, Y., 2008, "Tensile Properties of Ultrahigh Strength PAN-Based, Ultrahigh Modulus Pitch-Based and High Ductility Pitch-Based Carbon Fibers," Carbon, **46**, pp. 189–195.
[10] Sinclair, D., 1950, "A Bending Method for Measurement of the Tensile Strength and Young's Modulus of Glass Fibers," J. Appl. Phys., **21**, pp. 380–386.
[11] Oya, N., and Johnson, D. J., 1999, "Direct Measurement of Longitudinal Compressive Strength in Carbon Fibres," Carbon, **37**, pp. 1539–1544.
[12] Williams, W. S., Steffens, D. A., and Bacon, R., 1970, "Bending Behavior and Tensile Strength of Carbon Fibers," J. Appl. Phys., **41**, pp. 4893–4901.
[13] Jones, W. R., and Johnson, J. W., 1971, "Intrinsic Strength and Non-Hookean Behaviour of Carbon Fibres," Carbon, **9**, pp. 645–655.
[14] Curtis, G. J., Milne, J. M., and Reynolds, W. N., 1968, "Non-Hookean Behaviour of Strong Carbon Fibres," Nature, **220**, pp. 1024–1025.
[15] Da Silva, J. L. G., and Johnson, D. J., 1984, "Flexural Studies of Carbon Fibers," J. Mater. Sci., **19**, pp. 3201–3210.
[16] Hawthorne, H. M., 1993, "On Non-Hookean Behaviour of Carbon Fibres in Bending," J. Mater. Sci., **28**, pp. 2351–2535.
[17] Furuyama, M., Higuchi, M., Kubomura, K., Sunago, H., Jiang, H., and Kumar, S., 1993, "Compressive Properties of Single-Filamente Carbon Fibres," J. Mater. Sci., **28**, pp. 1611–1616.
[18] Oya, N., and Johnson, D. J., 2001, "Longitudinal Compressive Behaviour and Microstructure of PAN-Based Carbon Fibres," Carbon, **39**, pp. 635–645.
[19] Loidl, D., Paris, O., Bughammer, M., Riekel, C., and Peterlik, H., 2005, "Direct Observation of Nanocrystallite Buckling in Carbon Fibers Under Bending Load," Phys. Rev. Lett., **95**, p. 225501.
[20] Fukuda, H., Yakushijo, M., and Wada, A., 1999, "A Loop Test to Measure the Strength of Monofilaments Used for Advanced Composites," Adv. Compos. Mater., **8**, pp. 281–291.
[21] Naito, K., Tanaka, Y., Yang, J.-M., and Kagawa, Y., 2009, "Flexural Properties of PAN- and Pitch-Based Carbon Fibers, J. Am. Ceram. Soc., **92**, pp. 186–192.
[22] Francis, W. H., Lake, M. S., and Steven Mayes, J., 2006, "A Review of Classical Fiber Microbuckling Analytical Solutions for Use With Elastic Memory Composites," 47th AIAA/ASME/ASCE/AHS/ASC Structures, Structural Dynamics, and Materials Conference, Newport, RI, May 1–4, Paper No. AIAA-2006-1764.
[23] Francis, W. H., Lake, M. S., Schultz, M. R., Campbell, D., Dunn, M., and Qi, H. J., 2007, "Elastic Memory Composite Microbuckling Mechanics: Closed-Form Model With Empirical Correlation," 48th AIAA/ASME/ASCE/AHS/ASC Structures, Structural Dynamics, and Materials Conference, Honolulu, HI, April 23–26, Paper No. AIAA-2007-2164.
[24] Melanitis, N., Tetlow, P. L., Galiotis, C., and Smith, S. B., 1994, "Compressional Behaviour of Carbon Fibres. Part II: Modulus Softening," J. Mater. Sci., **29**, pp. 786–799.
[25] Daniel, I. M., and Ishai, O., 2006, *Engineering Mechanics of Composite Materials*, 2nd ed., Oxford University Press, New York.
[26] Trustum, K., and Jayatilaka, A. de S., 1979, "On Estimating the Weibull Modulus for a Brittle Material," J. Mater. Sci. **14**, pp. 1080–1084.
[27] Love, A. E. H., 1944, *A Treatise on the Mathematical Theory of Elasticity*, 4th ed., Dover, New York.
[28] Sanford, G., Biskner, A., and Murphey, T., 2010, "Large Strain Behavior of Thin Unidirectional Composite Flexures," 51st AIAA/ASME/ASCE/AHS/ASC Structures, Structural Dynamics, and Materials Conference, Orlando, FL, April 12–15, Paper No. AIAA 2010-2698.